Available online at www.sciencedirect.com
SCIENCE DIRECT®
Journal of Nuclear Materials 336 (2005) 314–322
journal of nuclear materials
www.elsevier.com/locate/jnucmat

Cross-sectional TEM and X-ray examination of radiation-induced stress relaxation of peened stainless steel surfaces

B.H. Sencer [a,*], G.S. Was [b,1], H. Yuya [c,2], Y. Isobe [d,3], M. Sagisaka [d,3], F.A. Garner [e,4]

[a] *Los Alamos National Laboratory, Materials Science and Technology (MST-8), P.O. Box 1663, MS-G755, Los Alamos, NM 87545, USA*
[b] *The University of Michigan, Materials Science and Engineering, Nuclear Engineering and Radiological Sciences, 2355 Bonisteel, Ann Arbor, MI 48109, USA*
[c] *Chubu Electric Company Inc., 20-1, Kitasekiyama, Ohdaka-cho, Midori-ku, Nagoya 459-8552, Japan*
[d] *Nuclear Fuel Industries Ltd., Noda 950, Kumatori-cho, Sennan-gun, Osaka 590-0491, Japan*
[e] *Pacific Northwest National Laboratory, Materials Resources, P.O. Box 999, Battelle Boulevard, P8-15 Richland, WA 99352, USA*

Received 21 April 2004; accepted 4 October 2004

Abstract

Neutron irradiation-induced relaxation was emulated using proton irradiation in order to determine the expected amount of stress relaxation in the peened surface layer of a BWR core shroud during its 40 year lifetime. Samples of 304 SS were shot peened to induce a compressive residual stress, and then irradiated with 3.2 MeV protons at 288 °C to four dose levels spanning 0.1–2.0 dpa. One set of specimens was as-peened and a second was pre-injected with 25 appm He. Depth-dependent measurements of internal stress were conducted using successive steps of X-ray line broadening measurement and electropolishing. Results showed that the compressive stress state was progressively relaxed, but was maintained at some level for the majority of the 2 dpa target dose. Helium pre-injection did not significantly affect the relaxation, but the magnitude of thermally-induced relaxation was somewhat greater, although it was observed to be largely a transient, saturable process. A new cross-section technique was developed that allows multiple observations to be made in one specimen at all depths, both in and beyond the peen-damaged range. The as-peened microstructure varies strongly with depth, consisting of deformation twins and dense dislocation networks. The radiation-induced relaxation on the microstructural level was expressed primarily in modification and reduction of the dislocation structure. A comparison was made between the proton-induced relaxation of internal stresses and predictions

* Corresponding author. Tel.: +1 505 664 0766; fax: +1 505 667 8021.
E-mail addresses: sencer@lanl.gov (B.H. Sencer), gsw@umich.edu (G.S. Was), yuya.hideki@chuden.co.jp (H. Yuya), sagisaka@nfi.co.jp (M. Sagisaka), frank.garner@pnl.gov (F.A. Garner).
[1] Tel.: +1 734 763 4675; fax: +1 734 647 7027.
[2] Tel.: +81 52 624 9466; fax: +81 52 624 9207.
[3] Tel.: +81 724 52 7221; fax: +81 724 52 7225.
[4] Tel.: +1 509 376 4136; fax: +1 509 376 0418.

0022-3115/$ - see front matter
doi:10.1016/j.jnucmat.2004.10.120

based on neutron-induced relaxation of externally-applied stresses. The relatively good agreement indicates that proton irradiation is a valid emulation of neutron irradiation for this application.

1. Introduction

Austenitic stainless steels employed as core internal materials in light-water reactors (LWRs) are susceptible to intergranular stress corrosion cracking (IGSCC) and irradiation-assisted stress corrosion cracking (IASCC). Cracking susceptibility is a function of the microstructure, the environment and the stress state. An important source of stress in core components is residual stresses arising from welding. Components under residual or applied stress undergo irradiation-induced relaxation in service [1,2].

The dose level required to completely relax a residual stress is of strong interest to design engineers. Although limited stress relaxation data are available from higher-flux fast reactors, there are very few data derived under lower-flux LWR irradiation conditions. In addition, there are essentially no data derived from compressive stress states, since most relaxation data are derived from either tensile, spring-shear or beam-bending conditions [2]. Such compressive stress states can be introduced in a specimen surface either by inadvertent damage or by deliberate peening, the latter performed to remove surface tensile stresses that might accelerate the formation of cracking. Such tensile stresses are known to arise during cooling in heat affected zones near welds.

The objective of this study was to evaluate the irradiation-induced stress relaxation of heavily cold-worked surfaces of 304 stainless steel specimens irradiated by high energy protons to emulate neutron irradiation of a BWR core shroud at a temperature of 288 °C. Proton irradiation has been used to successfully emulate neutron irradiation effects on radiation-induced segregation, microstructure, irradiation hardening and susceptibility to irradiation assisted stress corrosion cracking [3]. Also of interest was the effect of helium bubbles on irradiation creep and thereby stress relaxation, a mechanism of potential creep acceleration examined earlier by Garner and co-workers [4,5]. In water-cooled reactors the thermal-to-fast neutron ratio at steel–water interfaces is rather high, producing very high helium/dpa generation rates in stainless steels [6–8]. The issues of stress relaxation and its potential acceleration by bubble formation are also important to fusion reactors and accelerator-driven spallation neutron devices, both of which experience even higher helium generation rates [9–11].

Post-irradiation evaluation involved the use of X-ray stress measurement and transmission electron microcopy analysis. In addition to the proton irradiations, thermal annealing tests were conducted at the irradiation temperature for unirradiated specimens in order to estimate the possibly separate contributions of thermal relaxation and irradiation-induced stress relaxation.

2. Experimental procedure

2.1. Sample preparation and stress relaxation measurements

Commercial purity 304 stainless steel specimens with chemical composition listed in Table 1, were used in the solution annealed condition. The samples were prepared by electro-discharge-machine (EDM) to dimensions of $30.0 \times 4.0 \times 1.5$ mm, followed by peening on one surface to produce a compressive layer later measured in this study to be approximately 400 MPa just below the surface. The peening was carried out by blasting aluminum oxide powder (#150) onto the specimen surface at a pressure of 2.9 kPa for 5 s. The resultant root mean square surface roughness was 2–3 μm. The depth of peening damage was ~100 μm. Following peening, 25 appm He was pre-injected into one half of the peened specimens, using the procedure described later.

The surface residual stress measurement was conducted both before and after irradiation using an X-ray stress analyzer. Chromium X-radiation ($\mathrm{Cr\,K\alpha} = 0.22895$ nm; 40 kV, 30 mA) through a vanadium filter was used to examine the (220) peak for the 304 stainless steel.

The stress constant is used to calculate the residual stress distribution, which depends on the material. It can be calculated using Young's modulus and Poisson's ratio [10]. The stress constant employed was −620 MPa/deg and the size of the irradiated area examined on the specimen was approximately 2×4 mm. Such a measurement provides an average stress measurement over ~5 μm depth. In expectation that peened surfaces will exhibit heterogeneity on a very small scale the residual stress measurement for each sample was performed at least four times to obtain an average value, with the location of each measurement varying slightly. Portions of this irradiation study were published earlier [12] and the final results are presented in this paper.

Table 1
Chemical composition of the 304 stainless steel employed (wt%)

Alloy type	C	Si	Mn	P	S	Ni	Cr	Fe
304	0.058	0.51	1.12	0.030	0.004	8.80	18.35	Bal.

Some specimens were electropolished to provide access to an approximately 2×1 mm subsurface area of 20 μm depth. Subsequently it was possible to measure the average stress level of the 5 μm depth below the new surface.

2.2. Irradiation procedure

Proton irradiation and helium pre-injection were carried out using a tandem accelerator (General Ionex Tandetron) at the Michigan Ion Beam Laboratory for Surface Modification and Analysis at the University of Michigan. The pre-injection of helium was conducted by implanting 2.3 MeV He ions at a current of 150 nA while progressively tilting the specimen away from the beam normal according to a prescribed algorithm ($1/\cos\theta$), to produce a near-uniform helium distribution between 1 and 4 μm depth from the surface as shown in Fig. 1.

The distribution of helium with depth was calculated using the Microcal Origin™ computer program. The chosen upper dose of 2.0 dpa represents the maximum expected 40 year exposure in a typical BWR shroud at the beltline position.

The temperature rise due to beam heating during helium implantation was measured with a thermocouple to be ~100 °C. This introduces the possibility that beam heating and helium-generated displacements might contribute to the initial relaxation in the helium-implanted specimens.

The proton beam was raster-scanned over the specimen surface using a frequency of 255 Hz horizontal by 2062 Hz vertical. The damage profile calculated using the TRIM code shows that 3.2 MeV protons produce a relatively uniform (factor of ~2) damage profile over the first 25 μm of the proton's full range (42 μm). As shown in Fig. 2 there is a peak in dpa production starting gradually at 30 μm and extending to 42 μm. Fig. 3 summarizes schematically the depth profiles of the three surface altering processes, shot-peening, helium implantation and proton irradiation.

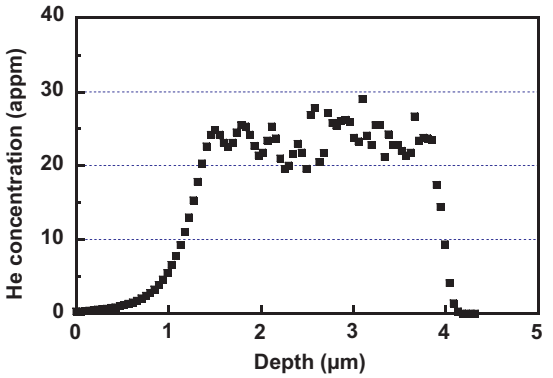

Fig. 1. Helium concentration as a function of depth calculated using the Microcal Origin™ program.

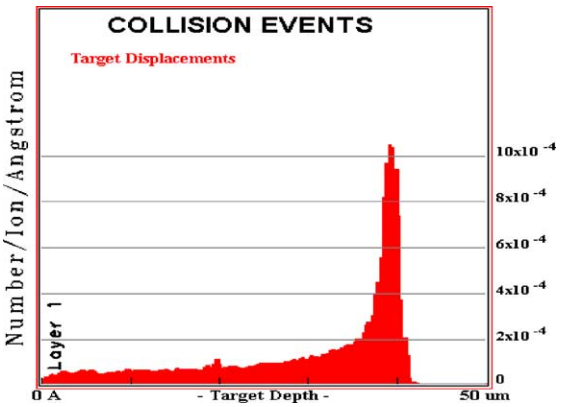

Fig. 2. Calculated 3.2 MeV proton damage profile using the TRIM code. Note that 3.2 MeV protons produce a relatively uniform (factor of ~2) damage profile over the first ~25 μm of the proton's full range (42 μm).

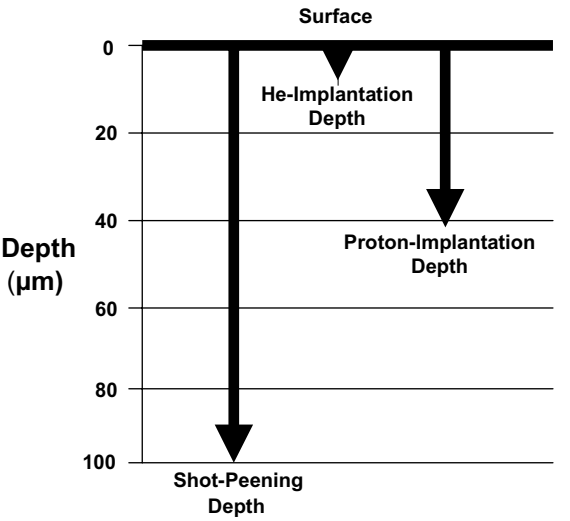

Fig. 3. Schematic illustration of the depth profiles of the three surface-altering processes: shot-peening, helium-implantation and proton-irradiation.

A displacement energy of 25 eV was used to calculate the dpa levels. The full range of the proton-damaged region is only ~40% of the peen-damaged layer, suggesting that significant irradiation-induced relaxation will probably not occur throughout the 100-μm damaged layer.

Two identical bars were irradiated side-by-side for each specimen condition and dose level. Thermal annealing tests on unirradiated specimens without

helium pre-injection were also conducted at 288 °C for periods ranging from 1 to 200 h in order to understand the difference in behavior between thermally-induced and irradiation-induced stress relaxation.

2.3. Post-irradiation analysis

Residual stress measurements and microscopy observations were carried out both before and after irradiation. Based on the residual stress measurements, the irradiation-induced stress relaxation of 304 stainless steels was evaluated. Transmission electron microscopy examinations were conducted with a TECNAI G2 (300 keV) in order to determine the mechanisms by which the relaxation was achieved. However, initial attempts to use conventional electropolishing techniques to produce electron-transparent foils were defeated by the large level of surface average roughness of 2.5 μm and the very large amount of stored energy in the peened volume.

To overcome this problem a cross-section technique was developed that allows multiple observations to be made in one specimen at all depths, both in and beyond the peen-damaged range. Two bars with nominally identical shot-peened surfaces were joined face-to-face with epoxy. These composite specimens were then machined to fit into a metal 5 mm tube, and then glued together with epoxy. The tube was sliced into sections ~600 μm thick using a diamond saw. A copper washer was then glued over the specimen for support against bending failure. Next, the diameter of the slice was reduced to 3 mm using a rotary saw. The specimen thickness was then reduced to ~40 μm by grinding using successively finer grades of grinding paper. The final surface polish was conducted using 1 μm diamond paste.

Two parallel rows of three dimples on each side of the peen-to-peen boundary were made with a mechanical dimpler, in order to increase the chance of successful thinning via subsequent ion milling. Polishing was performed on each dimple using 6 μm diamond paste. Final polishing was performed on each dimple using 1 μm diamond paste.

Gun angles used for ion milling with 5 keV ions were ±5–6° until perforation was achieved, followed by gun angles of ±3–4° with 2 keV ions to 'shave' the surface and remove any ion-induced damage introduced during earlier milling. The resulting hole in the composite specimen was elongated along the boundary and was very irregular in shape, allowing analysis at many positions along the boundary and at different depths from the peen-to-peen boundary as shown in Fig. 4.

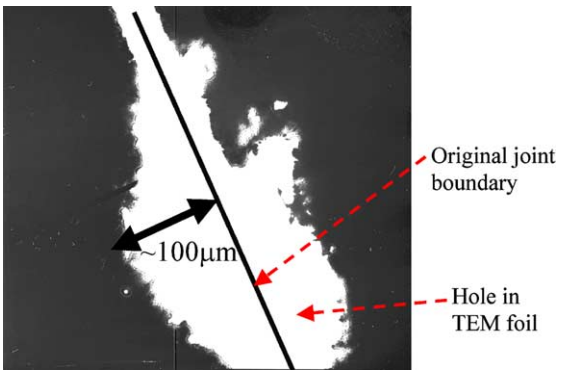

Fig. 4. Use of original joint boundary and irregular hole to determine the depth dependence of microstructure.

3. Results

3.1. Stress relaxation

The data shown in the following figures represent the average stress level comprising the first 5 μm of depth. The initial near-surface stresses for each original specimen were found to vary within ±60 MPa of 400 MPa. Fig. 5 shows the changes in near-surface residual stress relaxation induced by thermal annealing. It should be noted that the residual stress is calculated as the residual stress difference measured for the same specimen before and after the thermal annealing. The data shown in the following figures represent the average stress level comprising the first 5 μm of depth. The thermal annealing was performed in two different ways. In the first case, two as-peened samples were annealed in a furnace with nitrogen gas atmosphere for consecutive anneals totaling 1, 10, 100 and 200 h at 288 °C. In the second case, one as-peened sample was kept under vacuum at 288 °C for 50 h in the accelerator used for the proton

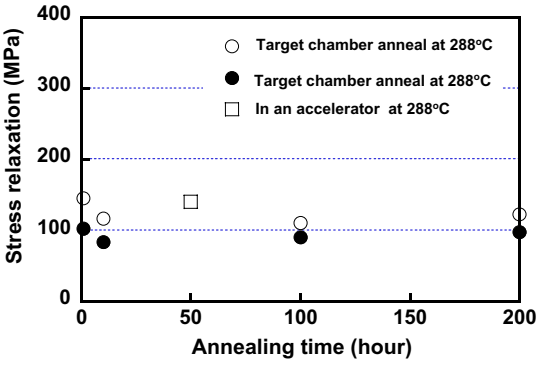

Fig. 5. Stress relaxation induced by thermal annealing at 288 °C. Two separate specimens were subjected to consecutive furnace anneals totaling 1, 10, 100 and 200 h, and the third specimen was annealed for 50 h in the tandem accelerator. (Note: original as-peened initial residual stress level ≈400 MPa).

irradiations. The results indicated that the thermally-induced relaxation near the surface saturates within one hour, reaching approximately 100 MPa relaxation of the compressive residual stress. This represents a near-immediate loss of ~25% (original as-peened initial residual stress level ≈400 MPa). It is reasonable to expect that in the original specimen condition the proximity of the surface will tend to reduce the compressive stress level compared to that at slightly greater depths. In one as-peened specimen (without helium) the first 5 μm showed an average compressive stress of 321 MPa with a measurement uncertainty/variation of ±69 MPa. Subsequent electropolishing of this specimen to reach 20 μm showed that the compressive stress in the 20–25 μm range was larger at 416 ± 55 MPa, thus demonstrating that the initial stress level is indeed larger away from the surface. A summary of the residual stress measurements at two different depths (5 and 20 μm) for protons and calculated creep relaxation for neutrons are given in Table 2.

The uncertainties quoted above probably reflect not only measurement accuracies but also the inherent position-dependent variability in stress level associated with such vigorous and small-scale heterogeneous deformation.

Fig. 6 shows the changes in residual stress induced by proton irradiation at 288 °C. Again, the residual stress shown is the difference measured for the same specimen before and after proton irradiation. Although the residual stress change also exhibits a tendency toward saturation, the relaxation is larger in magnitude than that induced by thermal annealing and is more prolonged in duration. Note that at the target dose of 2 dpa there is still about 100 MPa compressive stress maintained, which represents ~25% of the original stress level (original as-peened initial residual stress level ≈400 MPa).

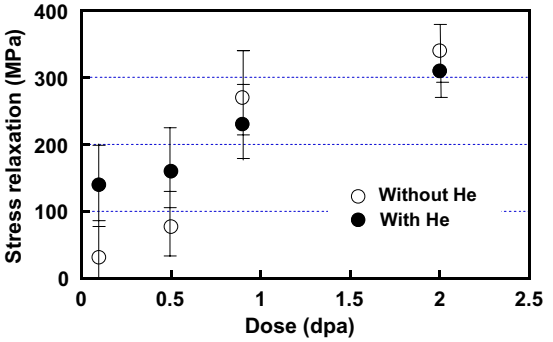

Fig. 6. Stress relaxation induced by proton irradiations including thermal relaxation. (Note: original as-peened residual stress level ≈400 MPa).

Creep relaxation prediction without a transient can be described as follows: $\sigma/\sigma_0 = \exp(-B_0 \times E \times \text{dose}/100)$, where σ_0 and σ are the residual stresses measured for the same specimen before and after the proton irradiation, respectively, and E is Young's modulus, and B_0 is the creep modulus [1,2]. If we employ for comparison a post-transient creep modulus, $B_0 = 1 \times 10^{-6}$ MPa^{-1} dpa^{-1}, derived from neutron irradiation studies [1,2], a comparison can be made between these results and earlier results from neutron irradiation.

Fig. 7 shows the fractional residual stress (σ/σ_0) as a function of dose for both the near-surface and below-surface measurements. Note that when compared with the neutron-based prediction, the proton irradiation results in a greater rate of relaxation with dose. However, both prediction and measurement display a similar post-transient dose dependence. Of course, transient creep is frequently observed during neutron irradiation as well,

Table 2
A summary of the residual stress measurements after proton irradiation (MPa) and the calculated creep relaxation predicted by neutron studies (MPa)

Dose (dpa)	Calculated creep relaxation for neutrons	Proton without He	Proton with He	Proton 20 μm depth without He	Without annealing		
					Proton without He	Proton with He	Proton 20 μm depth without He
0	1	1	1	1	1	1	1
0.1	–	0.92	0.67	–	1.17	0.92	–
0.2	0.96	–	–	–	–	–	–
0.4	0.92	–	–	–	–	–	–
0.6	0.89	0.79	0.63	–	1.04	0.88	–
0.8	0.85	–	–	–	–	–	–
0.9	–	0.41	0.39	–	0.66	0.64	–
1	0.82	–	–	–	–	–	–
1.2	0.78	–	–	–	–	–	–
1.4	0.75	–	–	–	–	–	–
1.6	0.72	–	–	–	–	–	–
1.8	0.69	–	–	–	–	–	–
2	0.67	0.24	0.19	0.37	0.49	0.44	0.61

Relaxation values are given as ratios (see Figs. 5–7).

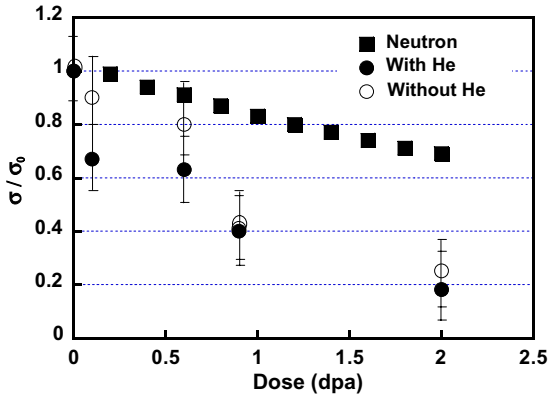

Fig. 7. Comparison of proton-induced relaxation (including thermal component) with the neutron-based prediction, the latter calculated only for the post-transient condition.

but in typical tensile tests the transient is not always very large, since the role of the surface in bulk specimens is not as strong as in the peened surface case [2].

Fig. 8 shows that when the thermally-induced relaxation of ~100 MPa is removed, however, the proton results are in relatively good agreement with the neutron-based predictions. The proton-induced transient appears to be only slightly larger than that produced by thermal annealing alone.

In order to determine the effect of depth on stress and proton-induced relaxation, a specimen without helium was examined after irradiation to 2 dpa. Over the first 5 μm the stress was compressive at 110 ± 48 MPa. After polishing to 20 μm depth the stress level was compressive and slightly larger at 156 ± 45 MPa. Thus the relaxation appears to proceed as expected at all depths reached by the proton beam. Based on irradiation creep theory, it is expected that the fractional relaxation per unit damage dose should be the same at all depths, independent of the original stress level [2]. This assumption can be tested using the two specimens discussed earlier (0 and 2 dpa) that were examined at both 5 and 20 μm. Assuming that the nominal average stress levels can be compared directly, the calculated residual stress ratios are 0.34 at 5 μm and 0.38 at 20 μm. Given the uncertainty in the measurements, this is considered to be rather good agreement.

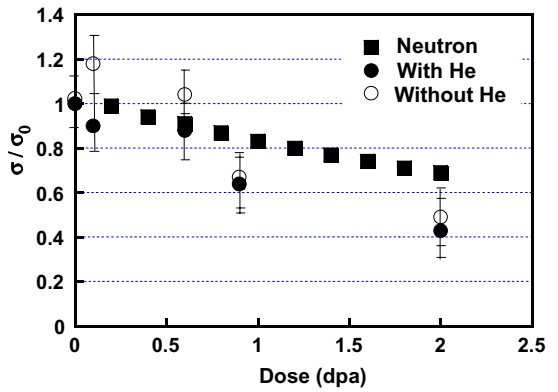

Fig. 8. Comparison of the neutron-based prediction with the proton-induced relaxation after removal of thermally-induced relaxation component.

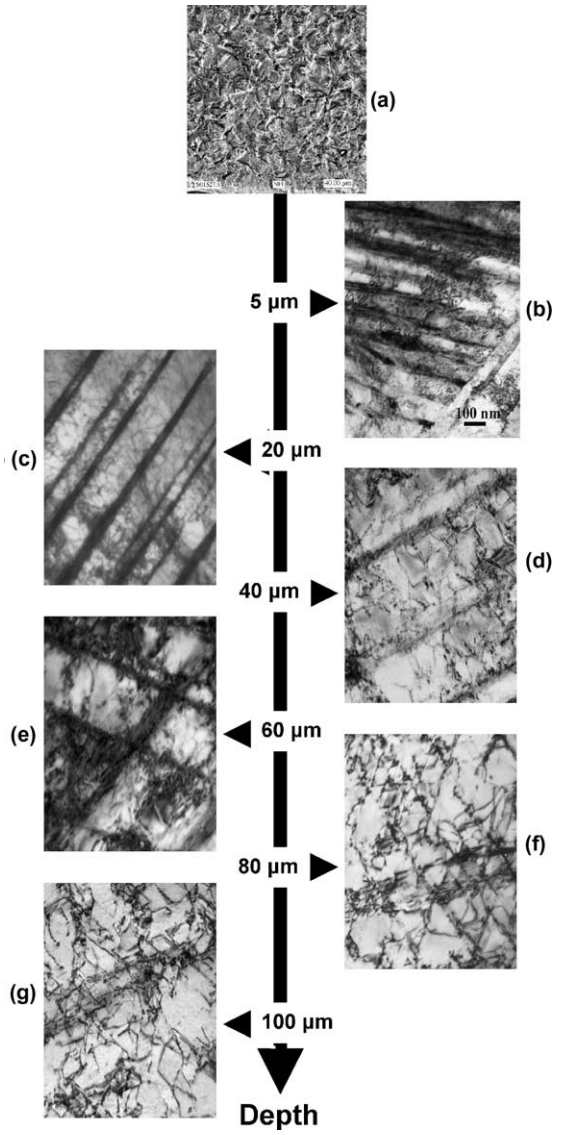

Fig. 9. Microstructure as a function of depth in the as-peened condition: (a) peened surface of AISI 304, showing 2–3 μm average roughness (SEM micrograph); (b)–(g) transmission electron micrographs.

3.2. Microstructural observation

The as-peened microstructure varies strongly with depth, consisting of deformation twins and very dense dislocation networks. Near the surface several slip systems were activated by peening to produce twin boundaries. Deeper from the surface less slip systems were found to be activated. The microstructure observed at different depths of as-peened 304 stainless steel is summarized in Fig. 9. Close to the shot-peened surface (5 μm) a heavily deformed microstructure is present consisting of deformation twinning and fine dislocations, with a high density of dislocations between twins, making it difficult to image individual dislocations. At 20–60 μm depth the microstructure is still heavily deformed (twinning density decreases and twin spacing increases with depth), but with twin and dislocation microstructure reduced in density such that individual dislocations are much easier to image. At ~80 μm, the dislocation microstructure and planar slip are clearly visible but twins are seldom observed. At ~100 μm, the microstructure is dominated by network dislocations.

Fig. 10 shows the microstructural change after 2 dpa without He pre-injection. In the regions where the proton-induced dpa profile is flat there are no dislocations, only a high density of loops. The twin structure is essentially unchanged, however. In the region where the proton-induced dpa is peaking, the dose is correspondingly higher; the loops are larger and have started unfaulting to produce a new dislocation network. The twin structure is still unchanged. The primary type of dislocation defect that evolved during irradiation was the faulted Frank loop which lies on {1 1 1} planes with 1/3 {1 1 1} Burgers vector. These loops produced distinctive satellite spots around the fundamental matrix spots in diffraction patterns. These satellite spots are called relrods and are associated with thin planar defects on {1 1 1} planes. The various satellite spots arise from extended diffraction streaks perpendicular to the four sets of {1 1 1} planes. The relrod technique and its application to microstructural characterization are described elsewhere [13]. Dark-field images of the loops taken with such streaks reveal the presence of faulted Frank loops, as shown in Fig. 11. The average

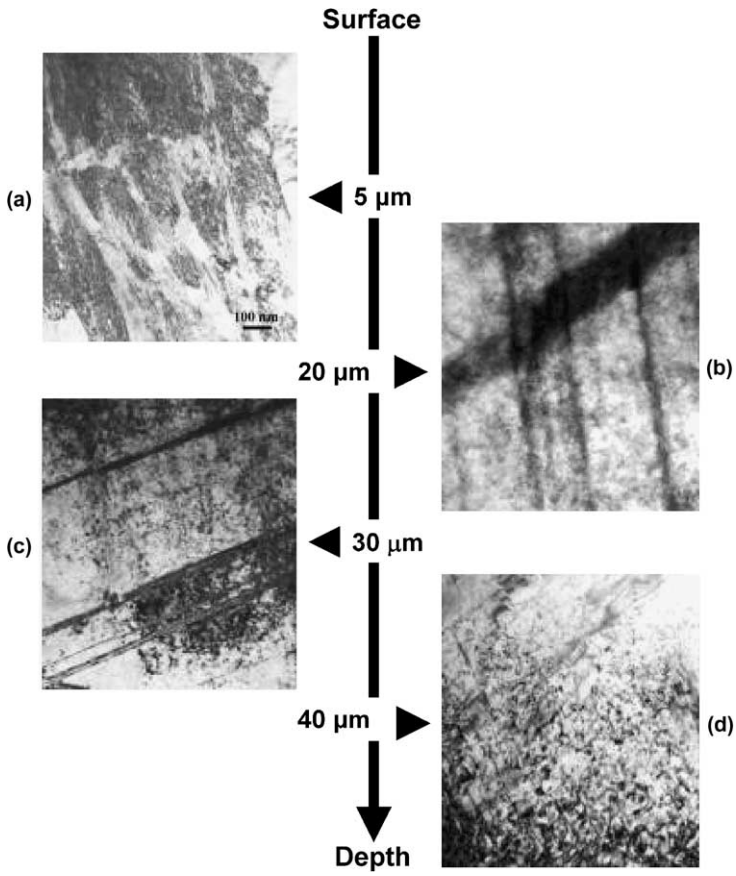

Fig. 10. TEM photos at different depths for the specimen at 2.0 dpa without helium pre-injection.

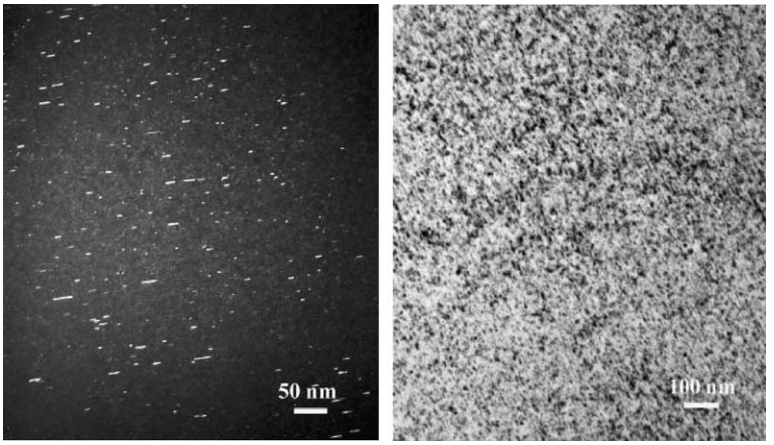

Fig. 11. TEM micrograph showing the rel-rod dark-field image (on the left) and the bright-field image (on the right) of faulted frank loops at the depth of 20 μm for the specimen at 2.0 dpa with helium pre-injection.

loop size is ~5 nm, while the average loop density is $\sim 9 \times 10^{22}$ m^{-3}.

4. Discussion

The results indicate that although ~70% of the average surface compressive stress induced by peening is relaxed during proton irradiation to 2 dpa, the compressive stress state is retained at the surface over an exposure level exceeding the maximum dose anticipated in any portion of a BWR core shroud over its 40 year lifetime. Approximately one third of the relaxation was thermally induced in the absence of irradiation. Although the original stress appears to vary with depth, the fractional relaxation of stress appears to be roughly independent of depth and associated stress level as expected.

Helium pre-injection to simulate the possible effect of bubble-accelerated creep did not significantly affect the relaxation, although the magnitude of thermally-induced relaxation appeared to be somewhat greater initially. However, it is thought that this somewhat larger initial relaxation may be a consequence of thermal relaxation occurring during the ~100 °C beam heating associated with the helium implantation process itself, especially since helium bubbles were not observed after irradiation and therefore could not contribute to the bubble-enhanced creep proposed by Woo and Garner [4].

Irradiation-induced relaxation at 2 dpa is most likely confined to the first ~42 μm, which corresponds to the near damage depth of the 3.2 MeV proton beam. Over the range 35–42 μm there must be a region of varying relaxation associated with the peak in dpa beyond the 35 μm depth, probably reaching near-zero residual stress at the damage peak about 40μm. Beyond >42 μm essentially no relaxation is expected. The interaction of the relaxed near-surface layers and the un-relaxed deeper volumes does not appear to lead to any reversal in surface stress, however. In the neutron case, of course, one would expect that the full peened depth would be equally relaxed with even less chance of stress reversal at the surface.

A comparison was made between the proton-induced relaxation of compressive and probably very complex internal stresses in the near-surface layer and predictions based on neutron-induced relaxation of externally-applied stresses. The agreement between the two cases confirms the theoretical expectation that the sign of the stress state is unimportant in determining the magnitude and kinetics of irradiation creep.

The rather good agreement between neutron-based predictions and the proton-induced relaxation indicates that proton irradiation is a valid emulation for this application. It is believed that for the purposes of stress relaxation there is no significant difference in effectiveness of proton-induced displacements and those produced by neutrons. Whereas it was earlier thought that, compared to neutrons, displacements induced by protons, electrons or gamma rays would be more effective in surviving recombination [13–16] and thereby cause more damage. More recent studies have shown that there appears to be no difference in displacement effectiveness, at least for relatively low temperatures experienced in BWR shrouds and pressure vessel walls [17–21].

5. Conclusions

- The as-peened damage layer for the specimens used in this study is ~100 μm deep, as confirmed by microscopy. There are significant changes in the peen-induced microstructure with depth.

- Proton irradiation of peened 304 SS at 288 °C to a dose of 2 dpa results in relaxation of approximately 75% of the 400 MPa initial residual stress.
- Of the ~300 MPa stress relaxation, about 100 MPa occurs due to nearly instantaneous thermally-induced relaxation at 288 °C.
- Taking into account the strong thermal relaxation arising from surface proximity, the agreement between neutron-induced predictions, and proton-induced relaxation data is remarkably good, indicating that proton irradiation can be used to emulate neutron irradiation-induced stress relaxation.
- Relaxation proceeds primarily by radiation-induced migration and subsequent reduction of the pre-existing dislocation network, concurrent with generation of small Frank loops. Deformation-induced twin boundaries appear to be largely unaffected by irradiation.
- The cross-sectional technique developed for this application successfully overcomes the thinning difficulties associated with microscopy of peened surfaces. The full depth dependence of microstructure is preserved in one specimen using this technique.

Acknowledgments

The authors are grateful to V. Rotberg and O. Toader for their help in conducting proton irradiation at the University of Michigan Ion Beam Laboratory. This research is supported by the Nuclear Fuel Industries Ltd. (NFI) of Japan. Additional support for the participation of F.A. Garner and the use of PNNL microscopy facilities by Sencer was provided jointly by the Materials Sciences Branch, Office of Basic Energy Sciences, and the Office of Fusion Energy, US Department of Energy. Pacific Northwest National Laboratory is operated by Battelle Memorial Institute under Contract DE-AC06-76RLO 1830.

References

[1] F.A. Garner, M.B. Toloczko, J. Nucl. Mater. 251 (1997) 252.
[2] F.A. Garner, Materials Science and Technology: A Comprehensive Treatment, vol. 10A, VCH, 1994, p. 419 (Chapter 6).
[3] G.S. Was, J.T. Busby, T. Allen, E.A. Kenik, A. Jenssen, S.M. Bruemmer, J. Gan, D.J. Edwards, P.M. Scott, P.L. Andresen, J. Nucl. Mater. 300 (2002) 198.
[4] C.H. Woo, F.A. Garner, J. Nucl. Mater. 271&272 (1999) 78.
[5] F.A. Garner, M.B. Toloczko, M.L. Grossbeck, J. Nucl. Mater. 258–263 (1998) 1718.
[6] F.A. Garner, B.M. Oliver, L.R. Greenwood, D.J. Edwards, S.M. Bruemmer, M.L. Grossbeck, 10th International Conference on Environmental Degradation of Materials in Nuclear Power Systems – Water Reactors, 2001, issued on CD format.
[7] F.A. Garner, L.R. Greenwood, B.M. Oliver, in: R.K. Nanstad, M.L. Hamilton, F.A. Garner, A.S. Kumar (Eds.), Effects of Radiation on Materials: 18th International Symposium, ASTM STP 1325, American Society of Testing and Materials, 1999, p. 794.
[8] F.A. Garner, L.R. Greenwood, D.L. Harrod, Proceedings of the Sixth International Symposium on Environmental Degradation of Materials in Nuclear Power Systems – Water Reactors, San Diego, CA, 1–5 August 1993, p. 783.
[9] F.A. Garner, B.M. Oliver, L.R. Greenwood, M.R. James, P.D. Ferguson, S.A. Maloy, W.F. Sommer, J. Nucl. Mater. 296 (2001) 66.
[10] F.A. Garner, L.R. Greenwood, Radiat. Eff. Def. Solids 144 (1998) 251.
[11] M. Kuroda, S. Yamanaka, K. Yamada, Y. Isobe, J. Alloys Comp. 314 (2001) 232.
[12] Y. Isobe, B.H. Sencer, G.S. Was, M. Sagisaka, H. Yuya, A. Nishikawa,Y. Sugita, F.A. Garner, 11th International Conference on Environmental Degradation of Materials in Nuclear Power Systems – Water Reactors, 2003, issued on CD format, p. 930.
[13] B.H. Sencer, G.S. Was, Y. Isobe, M. Sagisaka, G. Bond, F.A. Garner, J. Nucl. Mater. 323 (2003) 18.
[14] F.A. Garner, L.R. Greenwood, 11th International Conference on Environmental Degradation of Materials in Nuclear Power Systems – Water Reactors, 2003, issued on CD format, p. 887.
[15] F.A. Garner, L.R. Greenwood, P. Roy, in: R.K. Nanstad, M.L. Hamilton, F.A. Garner, A.S. Kumar (Eds.), Effects of Radiation on Materials: 18th International Symposium, ASTM STP 1325, American Society of Testing and Materials, 1999, p. 52.
[16] F.A. Garner, J.J. Laidler, in: Proceedings of Workshop on Correlation of Neutron and Charged Particle Damage, Oak Ridge, TN, 4 June 1976, p. 177.
[17] F.A. Garner, H.L. Heinisch, R.L. Simons, F.M. Mann, Radiat. Eff. Def. Solids 113 (1990) 229.
[18] D.E. Alexander, L.E. Rehn, J. Nucl. Mater. 217 (1994) 213.
[19] K. Farrell, S.T. Mahmood, R.E. Stoller, L.K. Mansur, J. Nucl. Mater. 210 (1994) 261.
[20] D.E. Alexander, L.E. Rehn, G.R. Odette, G.E. Lucas, D. Klingensmith, D. Gragg, in: Proceedings of 10th International Symposium on Reactor Dosimetry, Osaka, September 1999.
[21] D.E. Alexander, L.E. Rehn, G.R. Odette, G.E. Lucas, D. Klingensmith, D. Gragg, in: F.P. Ford, S.M. Bruemmer, G.S. Was (Eds.), Ninth International Symposium on Environmental Degradation of Materials in Nuclear Power Systems – Water Reactors, The Minerals, Metals & Materials Society (TMS), 1999, p. 827.